Phys Chem Minerals (2002) 29: 43–51
DOI 10.1007/s002690100204

ORIGINAL PAPER

A. Pavese

Pressure–volume–temperature equations of state: a comparative study based on numerical simulations

Received: 30 January 2001 / Accepted: 16 June 2001

Abstract The P–V–T equation of state (EoS) models of Birch–Murnaghan, Vinet and Poirier–Tarantola have been compared with one another and discussed in the light of their ability to reproduce thermoelastic functions and parameters by means of fitting to pressure–volume–temperature data artificially generated for spinel, corundum and forsterite. Numerical simulations relying upon semi-empirical potentials, lattice dynamics and the quasiharmonic approximation have been used to generate P–V–T data. The results obtained indicate that all the P–V–T EoSs tested predict bulk modulus at ambient conditions with errors confined, at worst, within a few percent, and reproduce correctly its dependence on temperature. The derivatives of the bulk modulus versus P and PT are less satisfactorily modelled. The bulk thermal expansion is determined by EoSs within a few percent error, but the deviations increase significantly if the approximation of linear dependence of EoS on temperature is used (linearised thermal pressure model).

Keywords P–V–T EoSs · Spinel · Corundum · Forsterite

Introduction

Pressure–volume–temperature equations of state (hereafter P–V–T EoSs) are a key to interpret a variety of mineralogical and petrological phenomena occurring in the natural environment, and provide access to many thermoelastic quantities which contribute in determining the equilibrium conditions of a phase alone or of an assemblage (Wallace 1972). For this reason, efforts are being directed to enhance the experimental stations in order to perform measurements at high-pressure and -temperature conditions to investigate P–V–T EoSs, as is confirmed by the increasing number of works on this subject issued in the last couple of years (for instance: Zhang et al. 1997; Wang et al. 1998; Xia et al. 1998; Fei et al. 1999; Morishima et al. 1999; Shinmei et al. 1999; Pavese et al. 1999; Dewaele et al. 2000; Shim et al. 2000; Shen et al. 2001).

However, many uncertainties still remain upon the theoretical models used to fit the observed P–V–T data and, in particular, on their ability to reproduce the thermoelastic parameters on which they are dependent. This is mainly due to the experimental difficulties encountered in performing high-pressure and -temperature measurements (see Duffy and Wang 1998 for a survey): (1) the precision in determining P and T (especially the former) in collecting P–V–T data varies with the extension of the accessible thermobaric range, which, in principle, should be as large as possible to allow one to reliably fix an EoS; (2) thermal and baric gradients impair the thermobaric homogeneity required to have ideal thermodynamic equilibrium, that is the condition for the EoSs to hold. Mezouar et al. (1999) and Dubrovinsky et al. (1999) (references therein) give an account of the performances of the presently available and most used high-pressure and -temperature cells (large volume cell equipped with a graphite heater and diamond anvil cell coupled to a laser heating system, respectively); Shen et al. (2001) discuss the recent enhancements in achieving thermal homogeneity in diamond anvil cells with laser heating.

In this light, numerical simulations, which are free of experimental drawbacks, can throw light upon the distortions affecting thermoelastic parameters inferred by EoS models from P–V–T data. We present here a comparative study of P–V–T EoSs organised as follows:

A. Pavese
Dipartimento di Scienze della Terra,
Università degli Studi di Milano, via Botticelli,
20133 Milano, Italy

National Research Council, Centro di Studio
per la Geodinamica Alpina e Quaternaria,
20133 Milano, Italy
e-mails: pavese@p8000.terra.unimi.it;
alessandro.pavese@unimi.it
Tel.: +39-02-23698321; Fax: +39-02-70638681

1. *P–V–T* data are generated by simulations, based on semi-empirical potentials, lattice dynamics and the quasiharmonic approximation, over the range 0–75 GPa and 300–1700 K.
2. The isothermal bulk modulus, its dependence on pressure and temperature, and the volume thermal expansion are analytically computed at each *P–V–T* point as described in the next section.
3. EoS models are fitted to the artificial *P–V–T* data and thermoelastic functions inferred.
4. Comparisons between points (2) and (3) are performed to assess the EoS models used.

Three compounds for which potentials are available have been investigated: forsterite (Pavese 1998), corundum (Catti and Pavese 1998) and $MgAl_2O_4$ spinel (Pavese, unpublished; potential function available from the author on request). The interest in these minerals is dictated by the fact that they have bulk modulus values covering a range (120–250 GPa at ambient conditions) common to most minerals of the Earth mantle.

We chose the range 0–75 GPa and 300–1700 K because, on one hand, it is representative of a thermobaric interval accessible for the investigation of *P–V–T* EoSs by experiments (see, for instance Table 2 of Duffy and Wang 1998) and, on the other hand, it is a range over which our method provides reliable results in terms of numerical stability. The present study is oriented to obtain insights into the reliability of some EoS models to determine thermoelastic parameters upon an experimentally possible *PT* range, rather than to compare EoSs analytically, for which purpose a wider *P* interval would be more appropriate in order to achieve extreme compressions (see, for instance Cohen et al. 2000). In this light, the present issues have to be considered with due care if the thermobaric range is significantly enlarged, or much softer materials are involved.

We have restricted our investigation to the *P–V–T* EoSs most used in the experimental mineralogical research, namely the Birch–Murnaghan model (Birch 1986), the Vinet model (Vinet et al. 1986, 1987) and the Poirier and Tarantola model (Poirier and Tarantola 1998); therefore in this presentation we do not deal with the Holzapfel EoS (Holzapfel 1996), the extended form of the Vinet EoS (Moriarty 1995; Vinet et al. 1989), the full form of the Jackson and Rigden thermodynamic model (Jackson and Rigden 1996) and the Kumar EoS (Kumar 1995; Kumar and Bedi 1996).

The present study joins and complements that of Vocadlo et al. (2000), devoted to the investigation of isothermal EoSs and their relations with the Grüneisen parameters.

Theoretical

Simulation method

The simulation method is outlined here; details are in Parker and Price (1989) and in Pavese et al. (1996).

The interaction energy between a pair of atoms r_{ij} apart is modelled by means of Born–Mayer-like potential functions, namely

$$E_{ij} = \frac{Q_i Q_j}{r_{ij}} + A_{ij}\exp(-r_{ij}/\rho_{ij}) - \frac{C_{ij}}{r_{ij}^6} \quad , \tag{1}$$

where the subscripts i and j indicate the chemical species involved in the interaction; Q (fractional charges), A, ρ and C are parameters determined by fitting theoretical to experimental quantities such as structural data, elastic constants and vibrational frequencies. Three-body interactions are also included to account for bond bending forces, and are described by an angular-type function as

$$E_{ijk} = \tfrac{1}{2}K_{ijk} \times (\theta_{ijk} - \theta_0)^2 \quad , \tag{2}$$

where θ_{ijk} is the angle between *i-j-k*, and θ_0 corresponds to its ideal value. The polarisation of oxygen is modelled by a shell model, assuming core and shell coupled with one another by a spring force.

The atomic coordinates and lattice parameters of a mineral are iteratively relaxed in order to achieve equilibrium with given P and T; this condition is fulfilled if

$$\frac{\partial G}{\partial \eta_j} = \sigma_j^{\text{ext}} \quad , \tag{3}$$

where G, is the Gibbs energy, η_j and σ_j^{ext} correspond to the jth component of the strain tensor and of the applied stress tensor, respectively. The first derivatives of G in Eq. (3) are split into a temperature-dependent contribution, numerically computed, and a temperature-independent part, analytically treated.

These calculations have been carried out by means of a home-adapted version (Pavese et al. 1996) of the PARAPOCS code (Parker and Price 1989), sampling 216 points throughout the **Q**-space.

EOS models

P–V–T EoSs can be thought of as extensions of *P–V* EoSs (isothermal EoSs). A *P–V* EoS is in general expressed as

$$P = P(V, V_0, K_0, K_0', K_0'') \quad , \tag{4}$$

where V_0, K_0, K_0' and K_0'' are the cell volume, bulk modulus, its first and second derivatives versus pressure at $P = 0$, and at a given reference temperature (T_0). Equation (4) can be turned into a *P–V–T* form by replacing V_0, K_0, K_0' and K_0'' with $V_0(T)$, $K_0(T)$, $K_0'(T)$ and $K_0''(T)$, which still give the corresponding quantities at $P = 0$, but at temperature T. Therefore Eq. (4) transforms into

$$P = P[V, V_0(T), K_0(T), K_0'(T), K_0''(T)] \quad . \tag{5}$$

The main limitations of such an approach are that it is dependent on which parametrization of $V_0(T)$, $K_0(T)$, $K_0'(T)$, $K_0''(T)$ one chooses, and that it neglects higher-order derivatives.

Alternatively, one can tackle the formalism of the *P–V–T* EoSs by splitting pressure into a static component (dependent on the strain only) and a thermal part (explicitly dependent on temperature). This means

$$P = P_0(V, V_0, K_0, K_0', K_0'') + \int_{T_0}^{T} \alpha K_T(T')\mathrm{d}T' \quad , \tag{6}$$

where α is the bulk thermal expansion, K_T the isothermal bulk modulus and $P_0(V)$ is the isotherm at a reference temperature (T_0), generally coinciding with ambient temperature. If $T \geq \Theta_D$, where Θ_D is the Debye temperature of the material under study, the integral of the right-hand side term of the equation above simplifies and Eq. (6) reduces to (Vinet et al. 1987)

$$P = P_0(V, V_0, K_0, K_0', K_0'') + \alpha_0 K_0 (T - T_0) \quad , \tag{7}$$

where α_0 is the bulk thermal expansion at T_0 and $P = 0$. Anderson and Isaak (1995) point out that Eq. (7) has been empirically proven

to maintain its validity at temperature by far lower than Θ_D. Jackson and Rigden (1996) discussed the general integration of Eq. (6) assuming a dependence on V and T of the αK_T term.

In the next section we deal with EoSs according to the Eqs. (5) and (6), adopting the approximation (7) for the latter. In the case of (7) we are mainly interested in estimating the distortions that such an approximation may cause on the thermoelastic parameters. The full Jackson–Rigden model is not discussed here because it is the subject of a specific study in progress.

For the sake of completeness, we report under P–V forms of the EoSs discussed in this study:

1. The Birch–Murnaghan EoS, resulting in:

$$P(V) = 3f_E(1+2f_E)^{5/2}\left(A + Bf_E + Cf_E^2\right) \ , \tag{8}$$

where $A = K_0$, $B = 3/2K_0(K_0' - 4)$ and $C = 3/2K_0[K_0K_0'' + (K_0' - 4)(K_0' - 3) + 35/9]$. f_E is the Eulerian strain defined as:

$$f_E = \frac{1}{2}\left[\left(\frac{V_0}{V}\right)^{2/3} - 1\right] \ . \tag{9}$$

2. The Vinet EoS, expressed as

$$P(V) = \frac{3K_0}{X^2}(1-X)\exp[\eta_0(1-X)] \ , \tag{10}$$

where

$$X = \left(\frac{V}{V_0}\right)^{1/3}$$

and

$$\eta_0 = \tfrac{3}{2}\left[K_0' - 1\right] \ .$$

3. The Poirier–Tarantola EoS, which is

$$P(V) = 3\tfrac{V_0}{V}f_N\left(A + Bf_N + Cf_N^2\right) \ , \tag{11}$$

where $A = K_0$, $B = 3/2K_0(K_0' - 2)$, $C = 3/2K_0[1 + K_0K_0'' + (K_0' - 2) + (K_0' - 2)^2]$ and

$$f_N = \frac{1}{3}\ln\left(\frac{V_0}{V}\right) \ . \tag{12}$$

Note that hereafter we use EoS to implicitly mean P–V–T EoS.

Results and discussion

A total of 220 P–V–T points for each compound have been simulated over the interval 0–75 GPa and along the isotherms at 300, 500, 700, 900, 1100, 1300, 1500 and 1700 K. Note that (1) the simulations predict thermobaric intervals of stability wider than the physical ones, and that (2) fitting parabolic expansions in f_E and f_N to the normalised pressures, i.e. $P/[3f_E(1+2f_E)^{5/2}]$ for the Birch–Murnaghan model and $P/[V_0/Vf_N]$ for the Poirier–Tarantola EoS, we observe second-order coefficients significant at least at the 100σ level. Point (2) proves that the thermobaric interval used is appropriate to fully fix the EoSs in study up to the fourth order of truncation; this is further confirmed by the small uncertainties affecting the inferred thermoelastic parameters shown in Table 1.

The results set out in Table 1 and discussed in this section have been obtained assuming the following parametrizations in Eq. (5):

$$K_0(T) = K_0 + K_0^T \times (T - T_0) \tag{13}$$

$$K_0'(T) = K_0' + K_0'^T \times \ln(T/T_0) \tag{14}$$

$$\alpha(T) = a_0 + a_1 \times T + a_2/T^2 \tag{15}$$

and

$$V_0(T) = V_0 \exp\left[\int_{T_0}^{T} \alpha(T')\mathrm{d}T'\right] \ . \tag{16}$$

Equations (16) and (13) are long-used parametrisations of the dependence of volume and bulk modulus on temperature; Eq. (14) has been suggested by Saxena and Zhang (1990), and Eq. (15) by Fei (1995). The χ^2 values reported in Table 1 have been calculated using a nominal uncertainty of 0.1 GPa on pressure. The THEO columns of Table 1 show the results of the simulations:

1. $K(P,T)$ (isothermal bulk modulus) and $\alpha(P,T)$ have been analytically calculated by structures equilibrated at given P and T according to the procedure in *Simulation method* (above). K_0 and α_0 correspond to $K(0,300)$ and $\alpha(0,300)$.

2. K_0' and K_0'' have been obtained as first and second derivatives of polynomials in P fitted to the calculated bulk modulus values (point 1) along the isotherm at 300 K. The polynomials in P have been truncated in order that their first and second derivatives versus pressure at $P = 0$ do not shift more than 3σ upon increasing the polynomial order.

3. a_0, a_1 and a_2 have been determined by fitting Eq. (15) to the analytically computed bulk thermal expansion values (point 1) along the isobar at $P = 0$.

4. $K_0'^T$ has been obtained by fitting Eq. (14) to the K_0' values obtained as explained above under (2) for each isotherm.

The thermobaric parameters of Eqs. (13), (14), (15) and (16) have been redetermined by fitting the EoS models of Birch, Vinet and Poirier–Tarantola to the P–V–T data from simulations.

The ability of the different EoSs investigated in reproducing the thermoelastic parameters is discussed in the following.

χ^2 assessment

The acronyms used below are explained in the caption of Table 1. The χ^2 values from the ABM3, ABM4, AV, APT3 and APT4 models (Eq. 7) are very sensitive to the refinement of V_0 in the case of corundum, while their dependence on V_0 decreases in spinel, and is practically negligible in forsterite. For BM3, BM4, V, PT3 and PT4 (Eq. 5), we did not attempt to refine V_0 in Eq. (16) because of the misleading correlations with the other parameters governing the dependence of volume on T via Eq. (15). In experiments the refinement of V_0 can account for 2θ-shift errors, but in the present case the data are free from any error of this sort; therefore V_0 acts here as an additional, but physically meaningless, degree of freedom which varies in order to minimise the

Table 1 Thermoelastic parameters of corundum, spinel and forsterite, determined by the EoS models discussed in the text. Expected standard deviations (1σ) are reported *in parentheses*. *THEO* corresponds to the results obtained by simulations; *BM3* third-order Birch–Murnaghan (i.e. $C = 0$ in Eq. 8); *BM4* fourth-order Birch–Murnaghan; *V* Vinet; *PT3* third-order Poirier–Tarantola (i.e. $C = 0$ in Eq. 11); *PT4* fourth-order Poirier–Tarantola. *ABM3*, *ABM4*, *AV*, *APT3* and *APT4* stand for the corresponding EoSs approximated according to Eq. (7). The *lower rows of the upper part* of the tables report the values obtained refining V_0. K_0 in GPa; K_0^T in GPa $K^{-1} \times 10^2$; K_0' is dimensionless; $K_0'^T$ in $K^{-1} \times 10$; K_0'' in $GPa^{-1} \times 10^2$; a_0 in $K^{-1} \times 10^6$; a_1 in $K^{-2} \times 10^9$; a_2 in $K \times 10$. $\chi^2 = 1/(N-M)\sum(P_{\text{theo}} - P_{\text{EoS}})^2/\sigma^2$ where N and M are the number of data and of parameters refined, respectively; $\sigma = 0.1$ GPa. $\Psi = \sqrt{\sum_{j=1}^{L}[\alpha_{\text{theo}}(T_j) - \alpha_{\text{EoS}}(T_j)]^2/L}$ where $L = 100$ is the number of points homogeneously sampled upon the interval from 300 to 1700 K

	Corundum					
	THEO	ABM3	ABM4	AV	APT3	APT4
K_0	245.7	243.1(4)	242.1(8)	241.9(4)	237.5(4)	242.4(9)
		247.7(5)	248.1(8)	246.5(5)	242.2(6)	248.2(8)
K_0'	4.74(1)	5.61(2)	5.8(1)	5.8(1)	6.57(3)	5.7(1)
		5.48(2)	5.43(8)	5.7(1)	6.38(3)	5.37(9)
K_0''	−1.9(4)		−4.3(5)			−3.5(7)
			−2.8(4)			−1.7(5)
α_0	15.70	23.4(1)	23.51(8)	23.5(1)	23.9(1)	23.5(1)
		23.6(1)	23.60(8)	23.7(1)	24.1(1)	23.6(1)
V_0	254.501					
		254.20(2)	254.20(2)	254.21(2)	254.22(3)	254.20(2)
χ^2		2.7	2.7	2.7	3.2	2.7
		1.6	1.6	1.6	2.3	1.6
	THEO	BM3	BM4	V	PT3	PT4
K_0	245.7	245.46(5)	244.9(1)	244.0(1)	238.1(5)	245.76(8)
K_0^T	−3.17(3)	−2.997(7)	−2.966(9)	−3.04(2)	−3.11(7)	−2.991(6)
K_0'	4.74(1)	5.500(3)	5.59(1)	5.690(6)	6.54(4)	5.43(1)
$K_0'^T$	3.1(8)	1.16(3)	0.39(2)	1.28(5)	2.5(3)	0.77(2)
K_0''	−1.9(4)		−3.64(8)			−2.09(8)
α_0	15.70	15.82	16.36	15.96	16.38	16.02
a_0	21.9(1)	22.17(8)	22.5(1)	22.1(1)	21.5(6)	22.31(6)
a_1	4.82(9)	4.41(6)	3.99(8)	4.6(1)	5.4(5)	4.24(4)
a_2	−7.0(1)	−6.9(1)	−6.6(2)	−6.7(2)	−6(1)	−6.81(9)
Ψ		0.25	0.43	0.13	0.37	0.31
χ^2		0.01	0.02	0.06	0.98	0.01

	Spinel					
	THEO	ABM3	ABM4	AV	APT3	APT4
K_0	207.6	207.0(4)	205.5(8)	205.6(4)	203.6(4)	205(1)
		205.3(6)	202(1)	203.5(6)	200.8(6)	202(1)
K_0'	3.80(2)	4.30(2)	4.5(1)	4.5(1)	4.83(2)	4.6(1)
		4.35(2)	4.7(1)	4.6(1)	4.94(3)	4.8(1)
K_0''	−3.2(2)		−3.2(5)			−3.8(7)
			−4.2(5)			−5.4(1)
α_0	14.1	20.0(1)	20.2(1)	20.2(1)	20.4(1)	20.2(1)
		19.9(1)	20.1(1)	20.0(1)	20.2(1)	20.2(1)
V_0	523.105					
		523.4(1)	523.5(1)	523.5(1)	523.6(1)	523.6(1)
χ^2		3.8	3.8	3.8	3.8	3.8
		3.6	3.4	3.5	3.4	3.4
	THEO	BM3	BM4	V	PT3	PT4
K_0	207.6	208.5(2)	205.2(2)	206.7(1)	204.1(2)	205.2(2)
K_0^T	−2.42(2)	−2.08(2)	−2.12(1)	−2.12(1)	−2.18(2)	−2.13(1)
K_0'	3.80(2)	4.338(8)	4.74(2)	4.559(6)	4.93(1)	4.78(2)
$K_0'^T$	3.2(3)	0.20(7)	−0.15(3)	0.39(5)	0.84(9)	−0.04(3)
K_0''	−3.2(2)		−4.2(1)			−5.0(2)
α_0	14.1	13.95	15.32	14.33	14.62	15.19
a_0	20.1(1)	20.5(4)	20.7(2)	20.3(2)	20.0(3)	20.6(2)
a_1	4.59(9)	3.6(3)	3.6(2)	3.9(1)	4.4(2)	3.7(1)
a_2	−6.6(1)	−6.9(6)	−5.8(4)	−6.4(3)	−6.1(4)	−5.8(3)
Ψ		0.68	0.63	0.45	0.20	0.57
χ^2		0.20	0.08	0.07	0.14	0.06

Table 1 (Continued)

	Forsterite					
	THEO	ABM3	ABM4	AV	APT3	APT4
K_0	127.3	128.1(1) 128.3(2)	126.3(2) 126.0(3)	126.3(1) 126.2(2)	123.2(2) 122.4(3)	126.1(3) 125.8(4)
K_0'	4.231(1)	4.545(7) 4.537(8)	4.83(3) 4.86(4)	4.85(7) 4.85(7)	5.48(1) 5.53(1)	4.88(4) 4.91(5)
K_0''	−7.9(1)		−5.8(2) −6.0(2)			−6.4(3) −6.7(4)
α_0	20.13	25.25(8) 25.2(1)	25.58(7) 25.58(8)	25.58(7) 25.56(8)	26.30(9) 26.2(1)	25.62(7) 25.62(8)
V_0	289.5894	289.54(4)	289.63(3)	289.62(3)	289.74(4)	289.63(3)
χ^2		0.6 0.6	0.5 0.5	0.5 0.5	0.8 0.8	0.5 0.5
	THEO	BM3	BM4	V	PT3	PT4
K_0	127.3	129.3(1)	126.6(1)	127.4(1)	123.6(3)	126.8(1)
K_0^T	−1.94(3)	−1.56(2)	−1.56(1)	−1.63(2)	−1.66(4)	−1.611(8)
K_0'	4.231(2)	4.493(8)	4.91(1)	4.796(7)	5.47(3)	4.89(2)
$K_0'^T$	6.6(7)	0.91(7)	0.14(2)	1.30(6)	2.4(3)	0.56(3)
K_0''	−7.9(1)		−6.6(1)			−6.9(2)
α_0	20.129	18.07	21.08	18.14	18.37	19.85
a_0	23.4(2)	24.3(6)	24.8(3)	24.1(4)	24(1)	24.6(2)
a_1	6.9(1)	5.0(5)	4.6(2)	5.9(3)	6.9(8)	5.2(2)
a_2	−4.8(2)	−7.0(9)	−4.6(5)	−6.9(6)	−6(1)	−5.6(3)
Ψ		1.48	1.24	0.84	0.44	0.87
χ^2		0.21	0.05	0.14	0.96	0.04

discrepancies between P predicted by EoSs [P_{EoS}] and P set [P_{theo}]. In this light, one reasonably expects that the more approximated the EoS model, the more marked its sensitivity to V_0. Corundum being the stiffest among the minerals examined in this study, small shifts of V_0 have remarkable effects on P_{EoS}, yielding significant changes of χ^2. These results suggest that particular care is required to treat V_0 when fitting an EoS of the type of Eq. (7) to experimental data, in keeping with issues of Cohen et al. (2000).

A decrease in the χ^2 values occurs using the BM3, BM4, V, PT3 and PT4 models, which is reflective of the crucial role of the dependence of the thermoelastic functions on T. In Fig. 1a–c we can compare the ability of Eq. (7) with that of Eq. (5) to fit each isotherm; we report, as an example, the results of the ABM3 (with both V_0 fixed and V_0 refined) and BM3 models. Using the ABM3 model with V_0 refined, the agreement between P_{EoS} and P_{theo} slightly improves throughout the thermal range studied with respect to the case with V_0 fixed, but the quality of the accordance becomes excellent if the BM3 model is considered. In Fig. 2a–c we discuss the ability of the BM4, V and PT4 models to reproduce P_{theo} along each isobar. The general agreement is good, and comparable between models; the largest deviations, that can be estimated at about 0.06 GPa, occur at the highest pressure values.

In short, we are able to reliably discriminate between models based on Eq. (7) and Eq. (5), but we cannot make a definitely unambiguous choice between BM3, BM4, V, PT3 and PT4, on the basis of χ^2 only.

K_0, K_0', K_0'', K_0^T assessment

Because of the above discussion, we will not consider in the following analysis the results obtained refining V_0.

Both ABM3-ABM4-AV-APT3-APT4 (Eq. 7) and BM3-BM4-V-PT3-PT4 (Eq. 5) are able to give K_0s which differ from the correct value by a few percent, and which are nearly coinciding in the case of BM3-BM4-V-PT4. The approximated EoSs (7) yield a slight underestimation of K_0. The largest deviations are due to the models based on the third-order truncation of the Poirier–Tarantola expansion (APT3 and PT3), although the discrepancy remains confined within 3%.

Two points are to be stressed as to K_0':

1. All the explored models yield overestimation of K_0'.
2. APT3 and PT3 give K_0' affected by the largest errors, whilst the other models lead to comparable first derivatives of the bulk modulus versus pressure. This point will be discussed.

The K_0'' values are reproduced [ABM4 (fixed V_0), APT4 (fixed V_0), BM4 and PT4 models] affected by errors ranging from a few percent up to 50%, and no rationale can be discerned. In particular, the large oscillations on K_0'' obtained by different EoSs hint that due care is to be paid in claiming precision in determining this elastic parameter. If we focus on the issues of BM4 and PT4, we observe that the discrepancies between the K_0'' values worked out are significantly larger than the uncertainties, except for the case of forsterite. This might reflect the fact that forsterite undergoes the largest compression

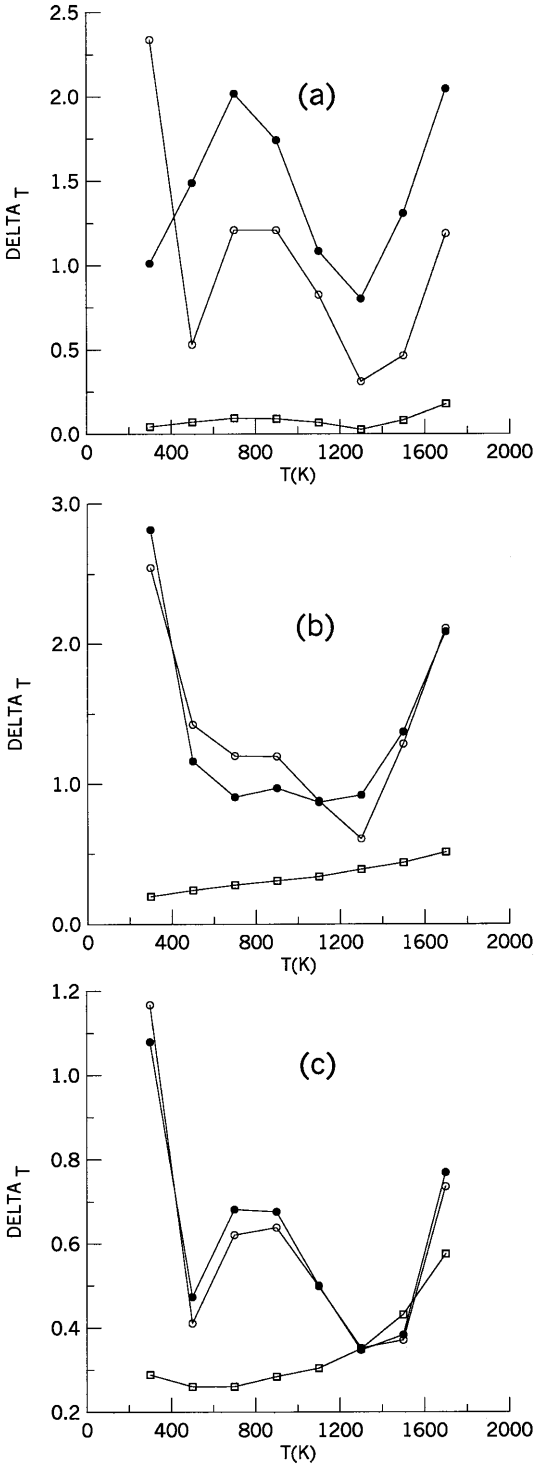

Fig. 1a–c $\Delta_T = 1/N_T \sum_1^{N_T} |(P_{\text{theo}} - P_{\text{EoS}})|/\sigma$ (N_T = number of points for the isotherm at T) is shown for corundum **a**, spinel **b** and forsterite **c** vs. T. *Filled circles* represent ABM3, with V_0 fixed; *empty circles* stand for ABM3 with V_0 refined; *empty squares* indicate BM3

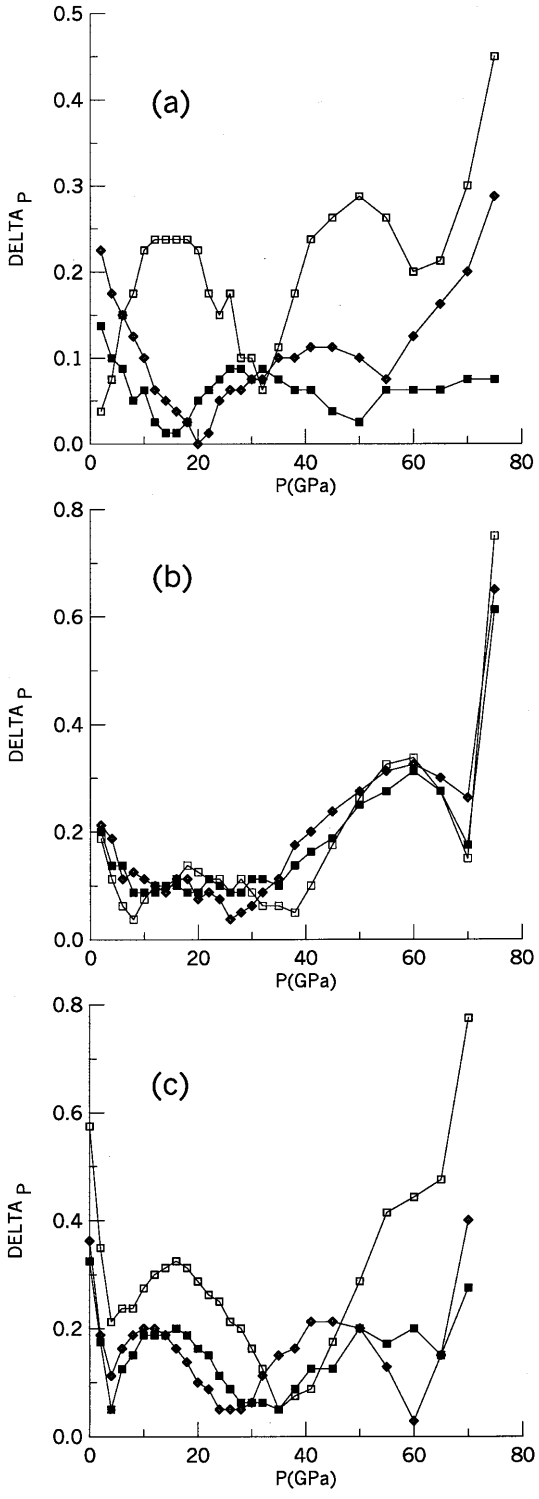

Fig. 2a–c $\Delta_P = 1/N_P \sum_1^{N_P} |(P_{\text{theo}} - P_{\text{EoS}})|/\sigma$ (N_P = number of points for the isobar at P) is shown for corundum **a**, spinel **b** and forsterite **c** vs. P. *Open diamonds* represent BM4; *empty squares* indicate V; *filled squares* PT4

and, therefore, it should be more sensitive to fourth-order truncations than corundum and spinel. This seems to be supported by the χ^2 values issued by BM4 and BM3 being, in the case of corundum, practically equal. Such an explanation, however, does not match the small uncertainties upon K_0'', which should be large if K_0'' was underdetermined. We believe the K_0'''s are skewed by (1) having neglected the dependence of K_0'' on T, and (2) K_0''

being the highest-order term of expansions in f_E or f_N, and therefore the one most affected by errors of truncation.

The APT4 and PT4 models systematically give K_0 and K_0' in better agreement with the correct values than APT3 and PT3, whereas the same does not hold for ABM4 and BM4, with respect to ABM3 and BM3. The Birch–Murnaghan model seems hence less sensitive to truncations than the Poirier–Tarantola EoS [compare BM3 issues with BM4s, and PT3s with PT4s; only for spinel do we have comparable differences of χ^2 between BM3-BM4 ($\approx$0.12) and PT3-PT4 ($\approx$0.08)]. In the case of corundum, for instance, the issues of PT4 approach PT3s if the baric interval is restricted to 30 GPa, that is $V/V_0 \approx 0.9$ according to the isotherm at 300 K.

K_0^T is reproduced with 5, 12 and 20% average error for corundum, spinel and forsterite, respectively. An analysis of the correlations between parameters reveals that K_0^T is strongly correlated with K_0, as expected. The larger K_0^T is the better the EoSs allow its determination, because of their sensitivity to $K_0(T)$.

Lastly, $K_0'^T$ is not well reproduced by the EoSs discussed. Such a result is presumably due on one hand to the low sensitivity of the EoSs to the mixed derivatives of the bulk modulus, and on the other to the probably poor parametrization of $K_0'^T(T)$ via Eq. (14). It is most likely that the precision in determining $K_0'^T$ may benefit from a wider *PT* range.

$\alpha_0, \alpha(T)$ assessment

The use of Eq. (7) (ABM3, ABM4, AV, APT3, APT4 models) leads to systematic overestimation of α_0, from about 25 to 50%. This is due to the partial inadequacy of Eq. (7) to describe the thermal dependence of EoSs. Note that the use of the extended Jackson–Rigden model yields improvement with respect to its approximation according to Eq. (7).

Adopting Eq. (5), one is able to satisfactorily retrieve the $\alpha(T)$ curve (see the issues of BM3, BM4, V, PT3 and PT4). BM3, BM4, V, PT3 and PT4 provide comparable $\alpha(T)$ curves (see Fig. 3a–c) that, in general, agree with the correct ones up to 1000 K (in particular for Al_2O_3 and $MgAl_2O_4$), while divergence occurs at larger T, though at 1700 K the discrepancies remain confined within 4% for corundum and spinel, and within 7% for forsterite. The best average accordance reveals in the range from 600 to 1000 K.

$K(P,T)$ prediction

One of the most ambitious aims of the EoSs is to predict the bulk modulus as a function of P and T, in order to allow modelling of the thermoelastic response of matter away from ambient conditions. In Fig. 4a–c one can assess how the PT4, V and BM4 models reproduce the $K(P,T)$ curve. We would like to draw attention to some aspects:

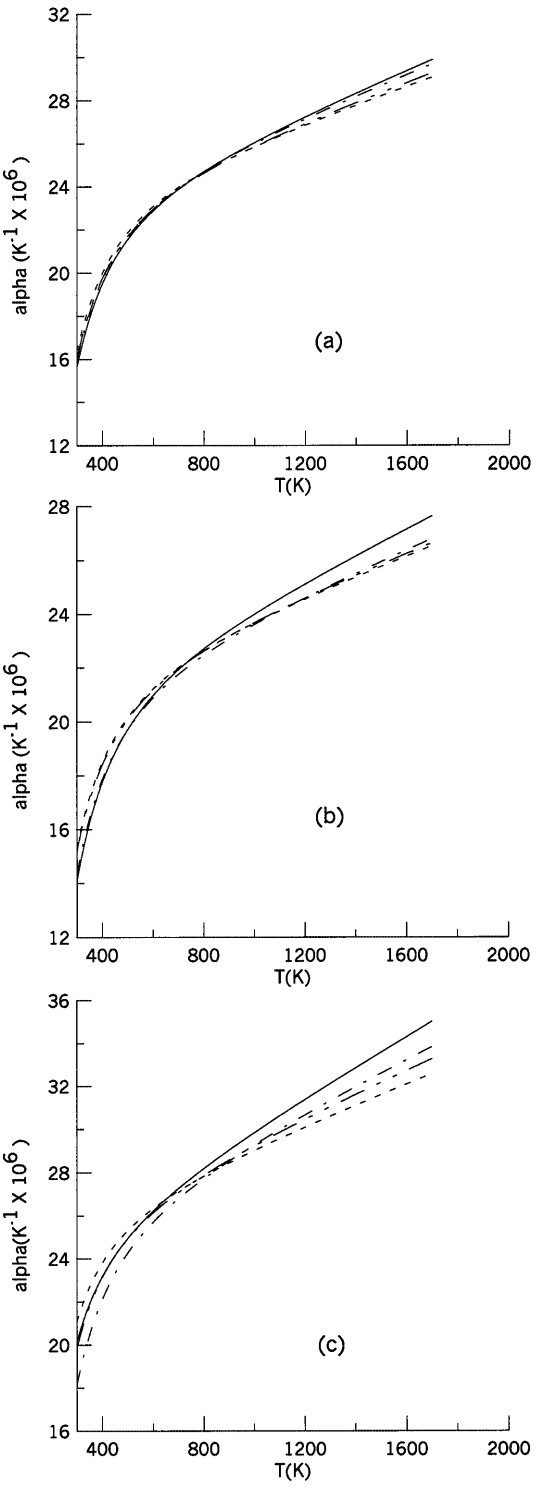

Fig. 3a–c Volume thermal expansion ($K^{-1} \times 10^6$) at room pressure as a function of temperature, for corundum **a**, spinel **b** and forsterite **c**. *Solid line* refers to calculated data; *dashed line* to the BM4 model; *dot-dashed line* to the V model; *dot-dot-dashed line* to the PT4 model

1. In general, the disagreement of BM4 and V with calculated $K(P,T)$ grows larger upon increasing pressure and temperature; this demonstrates the partial failure of

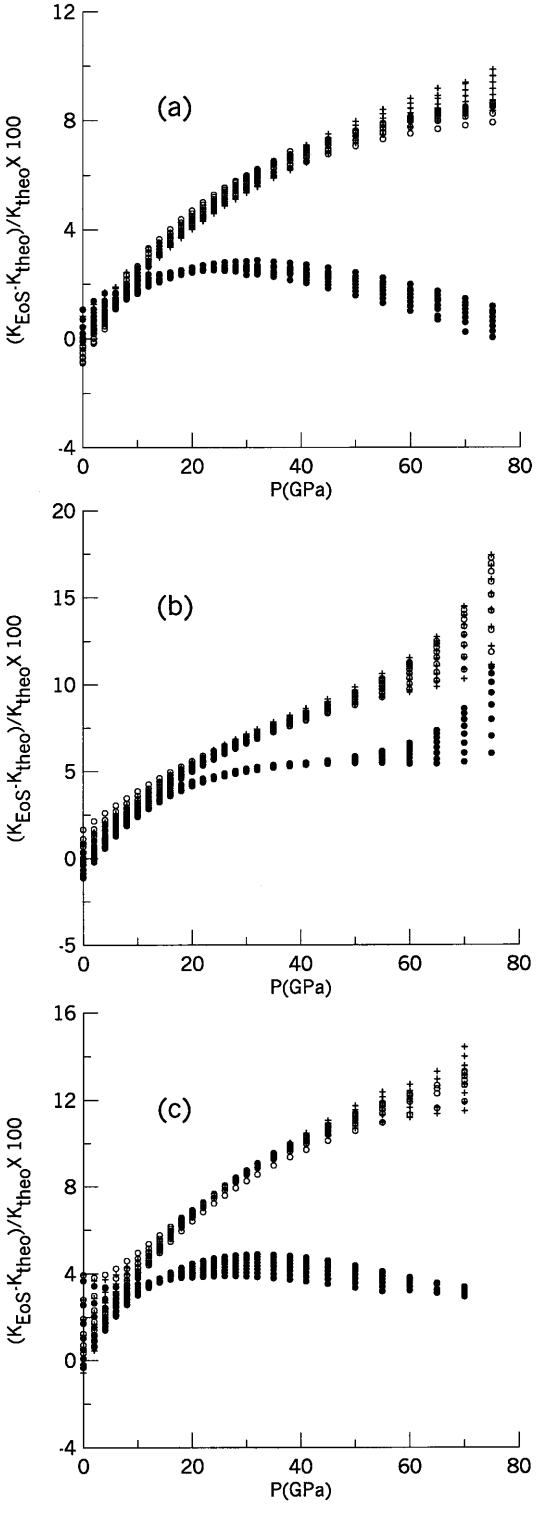

Fig. 4a–c $(K_{EoS} - K_{theo})/K_{theo} \times 100$ as a function of pressure (GPa), for corundum **a**, spinel **b** and forsterite **c**. *Filled circles*, *empty circles* and *crosses* refer to the PT4, V and BM4 models, respectively

these EoSs to model the bulk modulus in the high-pressure and -temperature regime.

2. While BM4 and V exhibit totally comparable ability to model-calculated $K(P,T)$, PT4 shows a significant improvement, leading to deviations confined within 10%, for spinel, and within 4% for corundum and forsterite.

The trends shown by the curves in Fig. 4a–c are reflective of the combination of a variety of effects: underestimation of $\alpha(T)$ in the high-temperature regime, deviation of K_0', K_0'', $K_0'^T$ and K_0^T from their correct values and analytic approximation of the P–V–T formulations.

Conclusions

On the basis of P–V–T data generated from 0 to 75 GPa and from 300 to 1700 K, for minerals with K_0 ranging from 130 up to 250 GPa, the following conclusions are drawn:

1. In terms of χ^2, the models of Eq. (5) are more satisfactory than those of Eq. (7); no definite choice can be made between BM3, BM4, V, PT3 and PT4. This is in keeping with Cohen et al. (2000), who report on P–V EoSs "for strain less than 30%, it probably does not matter what equation of state you use".

2. As to the bulk modulus and its derivatives versus P and T, all models give basically correct K_0s. In particular, the EoSs based on Eq. (5) yield bulk modulus in excellent agreement with the theoretical value, while the approximated EoSs (Eq. 7) give K_0 affected by slight underestimation. The accordance worsens progressively passing to K_0^T (≈12%), to K_0' (≈21%), to K_0'' (≈36%) and lastly to $K_0'^T$ (≈81%) (in brackets: average deviations from the correct values, according to the BM3, BM4, V, PT3 and PT4 models' issues). The expected precision to determine K_0^T and $K_0'^T$ after the method of Jackson and Rigden (1996) is 10 and 50%, respectively; the former is in fair agreement with our issue, whereas the latter results are better than ours, though possibly because of a poor parametrization $K_0'^T(T)$ used here. Note that the APT3 and PT3 models (i.e. third-order truncation of the Poirier–Tarantola EoS) give thermoelastic parameters affected by the largest errors. In general, the Poirier–Tarantola model is more sensitive than the Birch–Murnaghan EoS to truncations.

3. The use of Eq. (7) leads to overestimations larger than 25% of α_0, while the $\alpha(T)$ curve is retrieved within a few percent by Eq. (5). Deviations occurring in the high-temperature regime [≈1700 K] are still confined within 4% for corundum and spinel, and within 7% for forsterite.

4. V and BM4 predict similar bulk modulus values as a function of P and T, which exhibit increasing deviations from the calculated $K(P,T)$ curves upon increasing pressure. Such discrepancies are dependent on the minerals considered and, at worst, in the case of spinel, are about 15%. The PT4 model, instead, shows in general a remarkable ability in reproducing $K(P,T)$, and the disagreement does not exceed 10%.

Acknowledgements Financial support was provided by Italian MURST and CNR (Centro di studio per la dinamica alpina e

quaternaria, Milano). The author is indebted to M. Catti and G.D. Price, who reviewed the manuscript before submission.

References

Anderson OL, Isaak DG (1995) Elastic constants of mantle minerals at high temperature. In: Ahrens TJ (ed) Mineral physics and crystallography: a handbook of physical constants. Reference shelf 2, AGU

Birch F (1986) Equation of state and thermodynamic parameters of NaCl to 300 kbar in the high-temperature domain. J Geophys Res 91: 4949–4954

Catti M, Pavese A (1998) Equation of state of corundum from quasi-harmonic atomistic simulations. Acta Crystallogr (B) 54: 741–749

Cohen RE, Gülseren O, Hemley RJ (2000) Accuracy of equation-of-state formulations. Am Mineral 85: 338–344

Dewaele A, Fiquet G, Andrault D, Hausermann D (2000) P–V–T equation of state of periclase from synchrotron radiation measurements. J Geophys Res 105: 2869–2878

Dubrovinsky LS, Lazor P, Saxena SK, Haggkvist P, Weber HP, Le Bihan T, Hausermann D (1999) Study of laser-heated iron using third-generation synchrotron X-ray radiation facility with imaging plate at high pressure. Phys Chem Miner 26: 539–545

Duffy TS, Wang Y (1998) Pressure–volume–temperature equations of state. In: Hemley RJ (ed) Ultrahigh-pressure mineralogy. Mineralogical Society of America, Reviews in Mineralogy

Fei Y (1995) Thermal expansion. In: Ahrens TJ (ed) Mineral physics and crystallography: a handbook of physical constants. Reference shelf 2, AGU

Fei Y, Frost DJ, Mao H, Prewitt CT, Häusermann D (1999) In situ structure and determination of the high pressure phase of Fe_3O_4. Am Mineral 84: 203–206

Holzapfel WB (1996) Physics of solids under strong compression. Rep Progr Phys 59: 29–90

Jackson I, Rigden SM (1996) Analysis of P–V–T data: constraints on the thermoelastic properties of high-pressure minerals. Phys Earth Planet Int 96: 85–112

Kumar M (1995) High-pressure equation of state for solids. Physica (B) 212: 391–394

Kumar M, Bedi SS (1996) A comparative study of Birch and Kumar equations of state under high pressure. Phys Stat Sol 196: 303–307

Mezouar M, Le Bihan T, Le Godec Y, Libotte H, Thoms M, Häusermann D (1999) Paris–Edinburgh large-volume cell coupled with a fast imaging plate system for structural investigation at high pressure and high temperature. J Synch Rad 6: 1115–1119

Moriarty JA (1995) First-principles equations of state for Al, Cu, Mo and Pb to untrahigh pressures. High Press Res 13: 343–365

Morishima H, Ohtani E, Kato T, Suzuki A, Kikegawa T, Shimomura O (1999) The high-pressure and -temperature equation of state of a majorite solid solution in the system of $Mg_4Si_4O_{12}$–$Mg_3Al_2Si_3O_{12}$. Phys Chem Miner 27: 3–10

Parker S, Price GD (1989) Computer modelling of phase transitions in minerals. Adv Sol State Chem 1: 295–327

Pavese A (1998) Thermoelastic and structural properties of forsterite as a function of P and T: a computer simulation study, by semi-classical potentials and quasi-harmonic approximation. Phys Chem Miner 26: 44–53

Pavese A, Catti M, Parker S, Wall A (1996) Modelling of thermal dependence of elastic constants in calcite. Phys Chem Miner 23: 89–93

Pavese A, Ferraris G, Pischedda V, Mezouar M (1999) Synchrotron powder diffraction study of phengite 3T from the Dora Maira massif: P–V–T equation of state and petrological consequences. Phys Chem Miner 26: 460–467

Poirier JP, Tarantola A (1998) A logarithmic equation of state. Phys Earth Planet Int 109: 1–8

Saxena SK, Zhang J (1990) Thermochemical and pressure–volume–temperature systematics of data on solids, examples: tungsten and MgO. Phys Chem Miner 17: 45–51

Shen G, Rivers ML, Wang Y, Sutton SR (2001) Laser-heated diamond cell system at the advanced photon source for in-situ X-ray measurements at high pressure and temperature. Rev Sci Inst 72: 1273–1282

Shim SH, Duffy T, Shen G (2000) The stability and P–V–T equation of state of $CaSiO_3$ perovskite in the Earth's lower mantle. J Geophys Res 105: 25955–25968

Shinmei T, Tomioka N, Fujino K, Kuroda K, Irifune T (1999) In situ X-ray diffraction study of enstatite up to 12 GPa and 1473 K and equation of state. Am Mineral 84: 1588–1594

Vinet P, Ferrante J, Smith JR, Rose JH (1986) A universal equation of state for solids. J Phys (C): Sol Stat Phys 19: L467–L473

Vinet P, Smith JR, Ferrante J, Rose JH (1987) Temperature effects on the universal equation of state of solids. Phys Rev (B) 35: 1945–1953

Vinet P, Rose JH, Ferrante J, Smith JR (1989) Universal features of the equation of state of solids. J Phys: Cond Mat 1: 1941–1963

Vocadlo L, Poirier JP, Price GD (2000) Grüneisen parameters and isothermal equations of state. Am Mineral 85: 390–395

Wallace DC (1972) Thermodynamics of crystals. Wiley, New York

Wang YB, Weidner DJ, Zhang JZ, Gwanrnesia GD, Liebermann RC (1998) Thermal equation of state of garnets along the pyrope-majorite join. Phys Earth Plant Int 105: 59–71

Zhang J, Martinez I, Guyot F, Gillet P, Saxena SK (1997) X-ray diffraction study of magnesite at high pressure and high temperature. Phys Chem Miner 24: 122–130

Xia X, Weidner DJ, Zhao H (1998) Equation of state of brucite: single-crystal Brillouin spectroscopy study and polycrystalline pressure–volume–temperature measurements. Am Mineral 83: 68–74